



Tectonics

RESEARCH ARTICLE

10.1002/2017TC004710

Special Section:

An appraisal of Global Continental Crust: Structure and Evolution

Key Points:

- Multidisciplinary study of magmatic underplating and deep covered magmatic/fluid activity within new continental rift area
- Two types of magmatic emplacement with high-velocity reflective lower crust and high-velocity reflection-free magma body
- Different character of the underplated material responds to two episodes with different times of origin of underplating events

Correspondence to:

P. Hrubcová,
pavla@ig.cas.cz

Citation:

Hrubcová, P., Geissler, W. H., Bräuer, K., Vavryčuk, V., Tomek, Č., & Kämpf, H. (2017). Active magmatic underplating in western Eger Rift, Central Europe. *Tectonics*, 36, 2846–2862. <https://doi.org/10.1002/2017TC004710>

Received 30 JUN 2017

Accepted 21 OCT 2017

Accepted article online 4 NOV 2017

Published online 6 DEC 2017

Active Magmatic Underplating in Western Eger Rift, Central Europe

Pavla Hrubcová¹ , Wolfram H. Geissler² , Karin Bräuer³, Václav Vavryčuk¹, Čestmír Tomek⁴, and Horst Kämpf⁵
¹Institute of Geophysics, Czech Academy of Sciences, Prague, Czech Republic, ²Alfred Wegener Institute, Helmholtz Centre for Polar and Marine Research, Bremerhaven, Germany, ³UFZ Helmholtz-Centre for Environmental Research, Halle, Germany, ⁴Earth Science Institute, Slovak Academy of Sciences, Bratislava, Slovak Republic, ⁵GFZ German Research Centre for Geosciences, Potsdam, Germany

Abstract The Eger Rift is an active element of the European Cenozoic Rift System associated with intense Cenozoic intraplate alkaline volcanism and system of sedimentary basins. The intracontinental Cheb Basin at its western part displays geodynamic activity with fluid emanations, persistent seismicity, Cenozoic volcanism, and neotectonic crustal movements at the intersections of major intraplate faults. In this paper, we study detailed geometry of the crust/mantle boundary and its possible origin in the western Eger Rift. We review existing seismic and seismological studies, provide new interpretation of the reflection profile 9HR, and supplement it by new results from local seismicity. We identify significant lateral variations of the high-velocity lower crust and relate them to the distribution and chemical status of mantle-derived fluids and to xenolith studies from corresponding depths. New interpretation based on combined seismic and isotope study points to a local-scale magmatic emplacement at the base of the continental crust within a new rift environment. This concept of magmatic underplating is supported by detecting two types of the lower crust: a high-velocity lower crust with pronounced reflectivity and a high-velocity reflection-free lower crust. The character of the underplated material enables to differentiate timing and tectonic setting of two episodes with different times of origin of underplating events. The lower crust with high reflectivity evidences magmatic underplating west of the Eger Rift of the Late Variscan age. The reflection-free lower crust together with a strong reflector at its top at depths of ~28–30 km forms a magma body indicating magmatic underplating of the late Cenozoic (middle and upper Miocene) to recent. Spatial and temporal relations to recent geodynamic processes suggest active magmatic underplating in the intracontinental setting.

Plain Language Summary The Eger Rift, active element of the European Cenozoic Rift System, is associated with intense Cenozoic intraplate alkaline volcanism and system of sedimentary basins. The intracontinental Cheb Basin at its western part displays geodynamic activity with fluid emanations, persistent seismicity, Cenozoic volcanism, and neotectonic crustal movements at the intersections of major intraplate faults. In this paper, we study detailed geometry of the crust/mantle boundary and its possible origins. Based on seismic data from reflection and refraction profiles and from local seismicity, we identify significant lateral variations of the high-velocity lower crust and relate them to mantle-derived fluids and petrology. The observations point to a local-scale magmatic emplacement at the base of the continental crust within a new rift environment. The concept of magmatic underplating is evidenced by detecting two types of lower crust: a high-velocity lower crust with pronounced reflectivity and a high-velocity reflection-free lower crust. The character of the underplated material enables to differentiate timing and tectonic setting of two episodes with different times of origin of underplating events. Spatial and temporal relations to recent geodynamic processes suggest active magmatic underplating in the intracontinental setting.

1. Introduction

Magmatic processes play fundamental role in formation and differentiation of the Earth's crust. They are important for the evolution of the continental crust; however, their mechanisms still remain enigmatic. Increased P wave velocities, high V_p/V_s or Poisson's ratios, and high densities indicate a presence of mafic material in the lower crust (Christensen, 1996; Mooney et al., 1983). This suggests that large volumes of mantle-derived melts were emplaced at the base of the crust through a process called magmatic underplating (Furlong & Fountain, 1986). Magmatic underplating was originally inferred from petrology. Nowadays, mainly near-vertical or wide-angle reflections show evidence for ancient underplated material that ponded

around the base of the crust. It is observed in a variety of tectonic settings including island arcs, wide extensional continental areas, rift zones, continental margins, and paleo-suture zones (Thybo & Artemieva, 2013). Active magmatic underplating as a process of an ongoing magmatic activity at the lower crustal level is usually connected with lithospheric plate boundaries. However, it can also occur in intraplate setting (Jarchow et al., 1993), though it is a rare phenomenon not commonly observed or discussed.

The Eger Rift in Central Europe (Czech Republic, Germany, and Poland) is an active element of the European Cenozoic Rift System (ECRIS) (Prodehl et al., 1995). It is associated with an intense Cenozoic intraplate alkaline volcanism, a system of sedimentary basins, and rift shoulders at its northern and southern flanks (Andreani et al., 2014; Ulrych et al., 2011). At its western part, the small Cheb Basin is located, which is one of the unique European intracontinental areas. It displays concurrent present activity of geodynamic processes including CO₂ emanations and persistent seismicity. The CO₂-rich gases have ³He/⁴He ratios, which evidence their lithospheric mantle origin (Weinlich et al., 1999). The region is also characterized by Cenozoic/Quaternary volcanism and neotectonic crustal movements close to the intersection of major intraplate tectonic fault zones. Such geodynamic activities, fluids of lithospheric mantle origin, and earthquake swarms represent a unique phenomenon likely to be connected with a hidden ongoing deep-seated magmatic activity.

Active and passive seismic studies in the western Eger Rift indicate high *P* wave velocities at the base of the crust (DEKORP Research Group, 1994; Enderle et al., 1998; Hrubcová et al., 2005; Hrubcová & Geissler, 2009), sometimes with strong reflectivity or with a number of distinct reflective zones (Hrubcová et al., 2013; Hrubcová & Geissler, 2009; Tomek et al., 1997; Trappe & Wever, 1990). Lateral variations of the Moho in this area are reported by receiver function studies (Geissler et al., 2005, 2007; Heuer et al., 2006). Such results point to a tectono-magmatic modification and overprinting of the crust/mantle transition, though its detailed structure is still undisclosed.

In this paper, we review existing seismic and seismological studies of the crust/mantle boundary in the western Eger Rift. We provide new interpretation of the reflection profile 9HR and supplement it by new results from detailed imaging of the Moho retrieved from local seismicity. We detect significant lateral variations of the high-velocity lower crust and relate them to the distribution and chemical status of mantle-derived fluids and to xenolith studies from corresponding depths. We correlate the lateral lower crustal variations with tectonic regime and show that the observed phenomena point to the magmatic emplacement at the base of the crust and thus to a concept of magmatic underplating with different timing.

2. Western Eger Rift and the Cheb Basin

2.1. Tectonic Setting and Evolution

The Eger Rift belongs to the most prominent neotectonic structures in the Bohemian Massif, which is one of the largest stable outcrops of pre-Permian rocks in Central and Western Europe. This massif forms the easternmost part of the Variscan orogenic belt, which developed approximately between 500 and 250 Ma during a period of large-scale crustal convergence, subduction, collision of continental plates and microplates, and postcollisional extension (Matte et al., 1990). The westernmost part of the Eger Rift, the Cheb Basin, is situated in the junction of three different Variscan structural units (Franke, 2000): the Saxothuringian, the Teplá-Barrandian, and the Moldanubian (Figure 1). Babuška and Plomerová (2008) assume that these three lithospheric domains form a triple junction at the south-western end of the Eger Rift.

The Paleozoic suture between the Saxothuringian lithospheric segment in the north and the Teplá-Barrandian with the Moldanubian segments in the south has been reactivated repeatedly since the Eocene/Oligocene as a result of the Alpine collision (Ziegler, 1992). The extension during the Cenozoic together with alkaline magmatic activity led to the evolution of the Eger Rift, a 300 km long and 50 km wide ENE-WSW trending zone (Kopecký, 1978) as an active element of the ECRIS (Prodehl et al., 1995). This tectono-sedimentary structure is associated with a system of Cenozoic sedimentary basins and intense intraplate alkaline volcanism (Ulrych et al., 2011). Its alkaline character is dominated by rocks ranging from mellilitites, basanites, alkali basalts, ultramafic lamprophyres, and carbonatites to phonolites and trachytes with bimodal volcanism (Brandl et al., 2015). Three main episodes characterize the volcanic evolution of the Eger Rift: the prerift (79–49 Ma), the synrift (42–16 Ma), and the late-rift period (16–0.3 Ma). The initial Sr and Nd isotopic

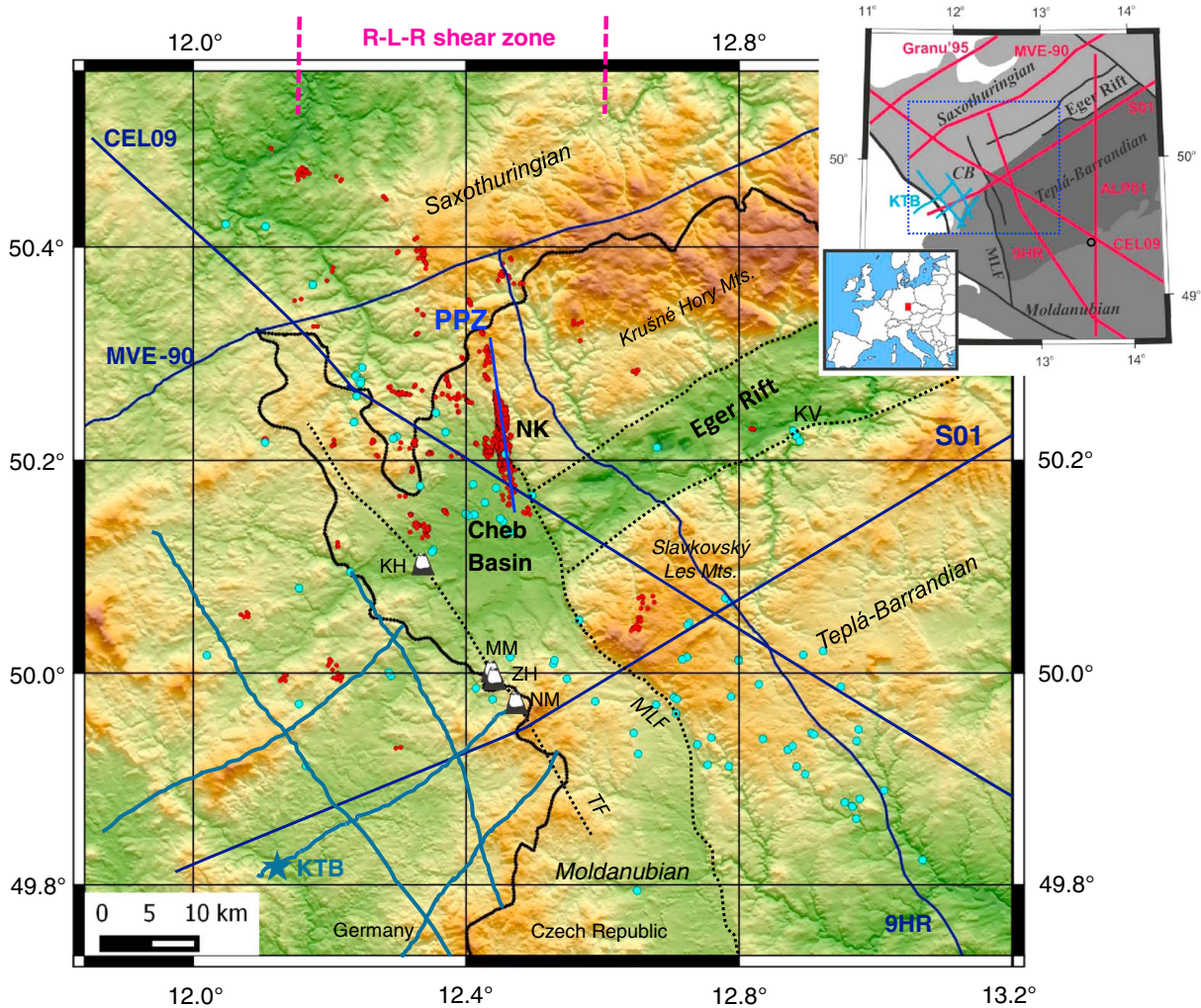


Figure 1. Western Eger Rift and the Cheb Basin. Seismic events of local swarm earthquakes in the period of 1995–2015 (double difference locations calculated by Hypo-DD; Bouchaala et al., 2013) are marked by the red dots; the distribution of degassing centers are marked by the cyan dots (Geissler et al., 2005); the seismic refraction/reflection profiles are marked by the blue lines. Four Quaternary volcanoes (KH, Komorní hůrka; ZH, Železná hůrka; MM, Mýtina Maar; NM, Neualbenreuth Maar) are indicated by the black/white cones. NK, the Nový Kostel focal zone; KV, Karlovy Vary spa region. MLF, Mariánské Lázně Fault; TF, Tachov Fault; R-L-R, Regensburg-Leipzig-Rostock Zone. The inset shows a superposition of the main tectonic units in West Bohemia with refraction/reflection seismic profiles marked by the red lines; the blue lines indicate reflection KTB profiles. CB, Cheb Basin.

ratios of the volcanic rocks are characteristic of magmas derived from a sublithospheric mantle source, similar to those of the European Asthenospheric Reservoir, and are ranked among the most depleted compositions in the ECRIS (Ulrych et al., 2016).

At the western part of the Eger Rift, the Cheb Basin of 265 km² is located at the intersection of the ENE-WSW striking Eger Rift and the NNW-SSE striking Mariánské Lázně Fault (MLF), part of the N-S trending Regensburg-Leipzig-Rostock Zone (Bankwitz, Schneider, et al., 2003). It is one of the unique European intracontinental areas displaying concurrent present activity of geodynamic processes. Originating from the reactivation of earlier Variscan faults in the basement, the Cheb Basin is filled with up to 300 m thick Cenozoic siliclastic sediment debris derived from the surrounding magmatic and metamorphic pre-Permian rocks, but it contains also material originating from shallow paleo-lakes and organic material. There is a gap in sedimentation from middle (17 Ma) to upper Miocene (4.7 Ma) (Rojik et al., 2014), which is possibly associated with volcanic activity of the late rift period (16–0.3 Ma) (Ulrych et al., 2011, 2016) and with the uplift of crustal blocks at the northern and southern shoulders of the Eger Rift (Andreani et al., 2014). On a wider regional scale, the position of the Cheb Basin is additionally controlled by an NS striking seismo-tectonic structure, the Regensburg-Leipzig-Rostock Zone (Bankwitz, Schneider, et al., 2003).

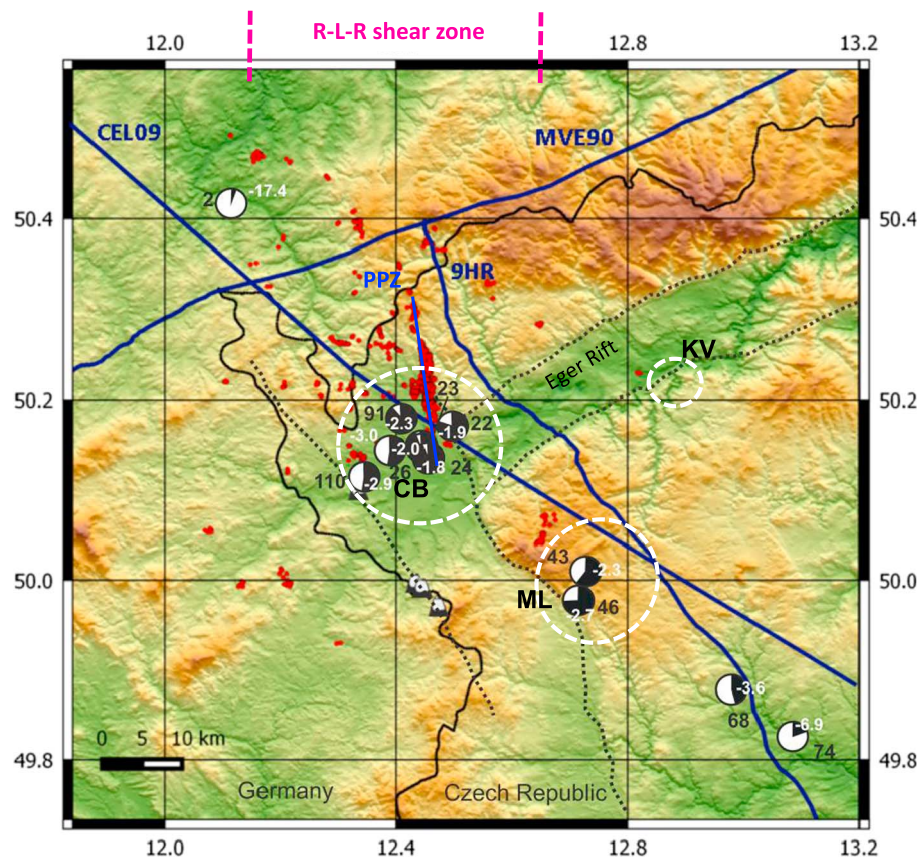





Figure 2. Helium and carbon isotope signatures of eight gas-rich mofettes. The black numbers represent the location numbers; the white numbers represent the $\delta^{13}\text{C}$ values. The black quarters of circles correspond to fractions of the mantle-derived helium corresponding to the subcontinental mantle reservoir with $^3\text{He}/^4\text{He} \approx 6.3 \text{ Ra}$ (Gautheron et al., 2005). All mofette sites were repeatedly sampled; data present mean values (after Bräuer et al., 2008, 2011; Kämpf et al., 2013). Based on a high gas flow, three degassing centers (CB, Cheb Basin; ML, Mariánské Lázně; KV, Karlovy Vary) are indicated with the white dashed circles (Weinlich et al., 1999). Seismic events marked by the red dots; four Quaternary volcanoes (KH, Komorní hůrka; ZH, Železná hůrka; MM, Mýtina Maar; NM, Neualbenreuth Maar) marked by the black/white cones. The dark blue lines correspond to seismic profiles. PPZ, Počátky Plesná Zone.

Late Cenozoic volcanic activity seems to be restricted to the western border of the Cheb Basin along the NW-SE striking Tachov fault, where four Quaternary volcanoes are known. There are two scoria cones, Komorní hůrka/Kammerbühl (KH) and Železná hůrka/Eisenbühl (ZH), and two maars, the Mýtina Maar (MM) (Flehsig et al., 2015; Mrlina et al., 2009) and a newly discovered Neualbenreuth Maar (NM) (Rohrmüller et al., 2017). The volcanism is dated 0.78–0.12 Ma ago (Mrlina et al., 2007; Ulrych et al., 2011, 2013; Wagner et al., 2002), whereas the onset of CO_2 -rich hydrothermal activity of the Karlovy Vary (KV) spa region (travertine deposit) is dated 0.23–0 Ma (Vylita et al., 2007). The eastern border of the Cheb Basin is formed by approximately 100 km long Mariánské Lázně Fault, morphologically expressed by a 50–400 m high escarpment intersecting the main seismoactive zone of Nový Kostel (NK; see Figure 1).

2.2. Present Geodynamic Activity

Present geodynamic activity in the Cheb Basin is manifested by recurrence of intraplate earthquake swarms and CO_2 emanations. The hypocenters of the events are located in the upper and middle crust down to about 20 km depth with the majority between 6 and 15 km and local magnitude less than 5 (Fischer et al., 2014). The seismicity is clustered in both space and time being monitored by seismic stations of the West Bohemian Network (WEBNET) (Horálek et al., 2000). It shows an episodic character and migration of hypocenters with the reactivation of previously ruptured fault segments (Vavryčuk et al., 2013). The most active part is the NK focal zone, where more than 80% of seismic energy was released within the last 35 years (Fischer et al., 2014; Vavryčuk, 1993). The trend of hypocenters in the narrow NNW striking belt and the source mechanisms are parallel to the N-S trending Počátky Plesná Zone (PPZ), part of the Regensburg-Leipzig-Rostock Zone (Bankwitz, Schneider, et al., 2003) (Figures 1 and 2).

Table 1
The Fluid Characteristics for the CB, ML, and KV Degassing Centers

	CB center	ML center	KV center
Gas flow (l/h)	>100,000	>100,000	>100,000
CO ₂ (vol %)	>99	>99	>99
Highest ³ He/ ⁴ He (Ra)	6.3	4.6	2.4
ESCM He (%)			

Note. ESCM, European subcontinental mantle.

The earthquake swarms occur close to CO₂-rich gas venting sites in mineral springs and mofettes (Figures 1 and 2); though, directly above the NK focal zone, the CO₂ degassing is extremely low. Based on a high gas flow, high CO₂ contents (>99 vol %), $\delta^{13}\text{C}$ values ranging between -2 and -4 ‰, and clear mantle-derived helium fractions, three degassing centers can be distinguished: the Cheb Basin (CB), Mariánské Lázně (ML), and Karlovy Vary (KV) (Geissler et al., 2005; Weinlich et al., 1999). The gas flow, CO₂ concentrations, $\delta^{13}\text{C}$ values, and ³He/⁴He ratios decrease from the degassing centers to their peripheries. The range of the carbon isotope signature among degassing centers is small; however, the fraction of mantle-derived helium differs substantially. The highest ³He/⁴He ratios were recorded in the CB center with up to 6.3 Ra; in the ML center it is up to 4.6 Ra, and in the KV center it is 2.4 Ra (where Ra = 1.39×10^{-6} corresponds to the atmospheric ³He/⁴He ratio) (Table 1). The large gas flow with $\delta^{13}\text{C}$ values close to mid-ocean ridge basalt (MORB) signature (Marty & Zimmermann, 1999) and clear mantle-derived helium fractions (Figure 2) point to the lithospheric mantle origin of the fluids supplied by an active degassing magma in the uppermost mantle (Bräuer et al., 2008, 2009; Kämpf et al., 2013).

3. Seismic Characterization of the Lower Crust

3.1. Previous Interpretations

The crust/mantle transition in the western Eger Rift area is characterized by a lower crustal layer with elevated *P* wave velocities of $6.9\text{--}7.5 \text{ km s}^{-1}$. It was detected along the refraction and wide-angle reflection profile CEL09 of the CELEBRATION 2000 experiment (Hrubcová et al., 2005) with a highly reflective top of the lower crust at a depth of 27–28 km as a characteristics of the Saxothuringian unit (Figure 3a). A high-velocity layer at the base of the crust was also found along deep reflection profiles MVE-90 (DEKORP Research Group, 1994), where the Moho was interpreted at 10 s two-way time at the bottom of a 5–6 km thick reflective lower crust (Figure 3b). The existence of a high-velocity lower crustal layer, with the top at 24 km and an average velocity of 7.0 km s^{-1} , was also indicated along the GRANU'95 refraction profile (Enderle et al., 1998) parallel with the MVE-90 profile more to the northwest. The Moho was interpreted at 10 s of two-way time corresponding to depths of ~32 km, where strong reflectivity dies out (Figure 3b). Similarly, increased velocities at the base of

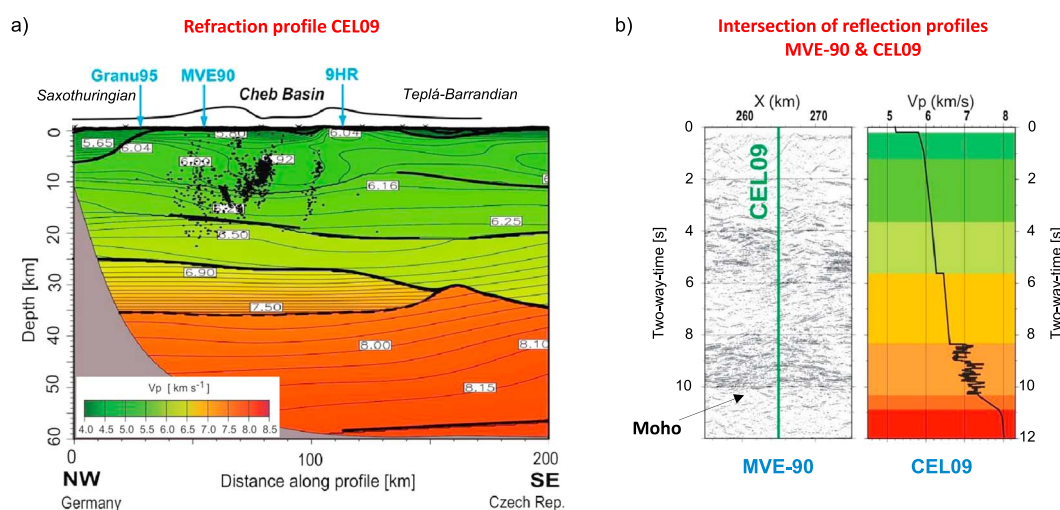


Figure 3. (a) High-velocity lower crust interpreted along the CEL09 refraction profile of the CELEBRATION 2000 experiment (after Hrubcová et al., 2005) with a highly reflective top of the lower crust at a depth of 27–28 km as a characteristic for the Saxothuringian unit. The grey covers the unconstrained parts of the model. Earthquakes are indicated by the black dots. (b) Increased reflectivity at the base of the crust along the MVE-90 reflection profile (DEKORP Research Group, 1994) with the 1-D velocity model from the refraction and wide-angle reflection profile CEL09 (converted to two-way time) at the crossing point (for the location, see Figure 1) (after Hrubcová & Geissler, 2009). Note the band of reflectors between 8.2 s and 10 s of two-way time at the MVE-90 profile corresponding to the high-gradient lower crust in the CEL09 profile. The Moho is interpreted at 10 s two-way time at the bottom of the 5–6 km thick reflective lower crust.

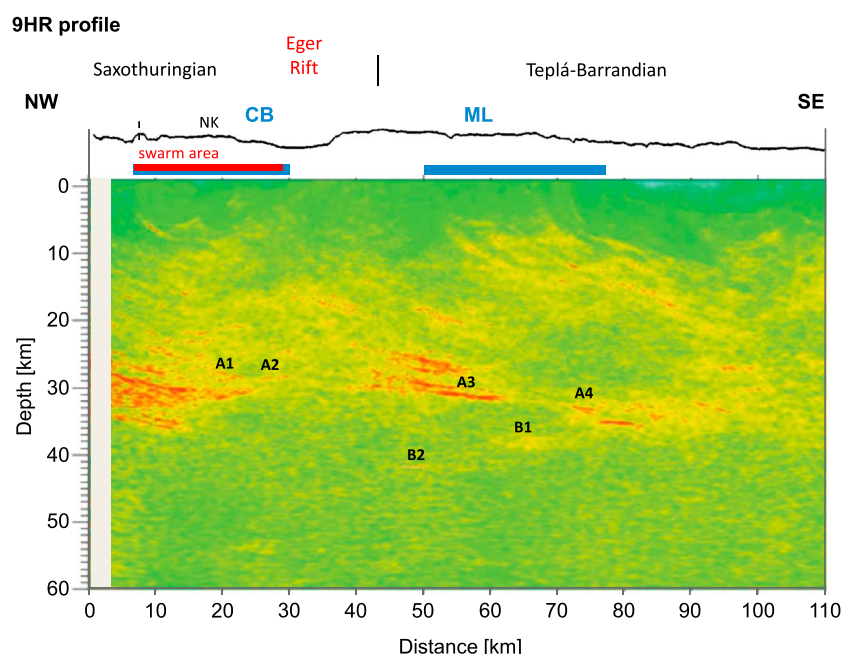


Figure 4. Reprocessed Kirchhoff prestack section of the northwestern part of the 9HR reflection profile (after Mullick et al., 2015) depth migrated with a 1-D velocity profile of Málek et al. (2005). Degassing centers CB and ML are labeled. Note an abrupt termination of the seismic reflectivity at 14 km along the profile. The reflectors at the top of the lower crust at depths of 28–30 km with a missing reflectivity below are traced at a distance of 14–75 km (labels A1, A2, and A3) terminating at a depth of 32 km (reflector A4). Deeper reflectors at depths of 37 and 41 km at distances of 45 and 75 km (labels B1 and B2) dip northwest and represent a bottom delimitation of the lower crust, the Moho. The blue bars represent the extent of the CB and ML degassing centers at the surface; the red bar represents the extent of seismicity projected at the surface. NK, the Nový Kostel focal zone.

the crust were identified at the S01 refraction profile of the SUDETES 2003 experiment (Grad et al., 2008), and at the ALP01 profile of the ALP 2002 experiment (Brückl et al., 2007) (Figure 1). This is in agreement with the result of joint modeling of receiver functions and the refraction CEL09 profile beneath the Cheb Basin by Hrubcová and Geissler (2009), who confirmed lower crustal layer (or gradient zone) to be 4–5 km thick with its top at a depth of 28 km where high reflectivity obscured weak Moho reflections from depths of ~32–33 km. The seismic reflection profile 9HR indicated a strong reflector at 9.2 s of two-way time beneath the Eger Rift, while Moho was interpreted at the bottom of the reflective zone at ~35 km (Tomek et al., 1997). This profile also imaged a reflector in the uppermost mantle beneath the rift axis at a depth of 56 km interpreted with the layers of eclogite or garnet pyroxenite. A zone of increased reflectivity at the base of the crust was also mapped along the DEKORP reflection profiles near the deep drilling site KTB with continuation to the northeast toward the Czech/German border (DEKORP Research Group, 1988; Trappe & Wever, 1990) (see Figure 1).

3.2. New Interpretation of 9HR Reflection Profile

The seismic reflection profile 9HR runs in the NW-SE direction and passes close to the main focal zone NK and the degassing fields (Figure 1). It is 200 km long and it starts at the Czech/German border and terminates in southern Bohemia. The profile was realized with dynamite sources at 20 m deep drillholes, the split-spread geometry, the maximum offset of 5 km on each side of the shot points, and a shot and geophone spacing of 200 m and 50 m, respectively. Total recording length was 24 s with a sampling interval of 4 ms. Acquired in early 1990s, it was processed with poststack migration technique (Tomek et al., 1997). Later, its 150 km northwestern part was reprocessed by the Kirchhoff prestack depth migration and the seismic image was discussed for its upper crustal structures (Mullick et al., 2015). However, its deeper parts and the crust/mantle boundary have not been interpreted in detail.

The northwestern part of the reprocessed Kirchhoff prestack section of the 9HR profile (Mullick et al., 2015) migrated with 1-D velocities of Málek et al. (2005) is shown in Figure 4. The seismic image reveals a reflective lower crust pronounced in the northwest (at distances of 0–14 km) at depths of 27–35 km with the Moho interpreted at its bottom (see also Tomek et al., 1997; increased reflectivity and reflector M_1). However,

from a distance of 14 km toward the southeast, the lower crustal reflectivity is missing and only strong reflectors with lateral variations in their intensity are visible at the top of the lower crust at depths of ~28–30 km (reflectors A1, A2, and A3) (see also Tomek et al., 1997; reflectors B). Similar character can be traced up to a distance of 75 km along the 9HR profile terminating at a depth 32 km (reflector A4). Between the distances of 45 km and 75 km, deep reflectors can be identified at depths of ~37–41 km (reflectors B1 and B2) (see also Tomek et al., 1997; reflectors MR₁ and MR₂). These reflectors dip northwestward and most probably represent the bottom delimitation of the lower crust, i.e., the Moho as the boundary between the crust and mantle materials. Seismic velocities above and below these reflectors can be inferred from the results of Hrubcová et al. (2005), who interpreted the Moho as a thin (about 1 km) layer with the velocity increase from 7.5 to 7.9 km s⁻¹ at a depth of 34–36 km, and the velocities in the lower crustal layer in a range of 6.9–7.5 km s⁻¹. This was also confirmed by joint modeling of receiver functions and the refraction CEL09 profile beneath the Cheb Basin by Hrubcová and Geissler (2009). To conclude, high velocities in the lower crust, the absence of a reflectivity, and the reflectors at the top and bottom delimit a high-velocity lower crustal body located between distances of 14–75 km along the 9HR profile.

The delimitation of the high-velocity body in the lower crust is not equally visible at all distances. At distances of 22–43 km along the 9HR profile, the reflector at the base of the lower crust (the Moho) is missing. Thus, the only reflector is at the top of the lower crust (A1). As a consequence, Tomek et al. (1997) discussed this reflector as a possible crust/mantle boundary. In a similar way, Geissler et al. (2005) and Heuer et al. (2006) interpreted the only pronounced interface from teleseismic receiver functions as the Moho with its elevation beneath the Cheb Basin (see Figure 1). However, from the results of Hrubcová et al. (2005), the velocities below this interface are in a range of 6.9–7.5 km s⁻¹ being distinctly lower than mantle velocities (>7.9 km s⁻¹). Thus, this reflector should not be the Moho, but rather the top of the lower crust. Note that lower amplitude of the less visible reflections at distances of 29–35 km along the 9HR profile can be partly explained by lower data resolution and technical difficulties in the 9HR data acquisition (missing shot points and high seismic noise in the area of the Eger Rift) and partly by attenuation of energy in sediments in the uppermost crust (sedimentary basins).

3.3. New Details of the Lower Crust From Local Seismicity

To confirm the geometry of reflective zones at the lower crustal level identified in the 9HR data, we additionally processed data from local seismicity that occurred beneath the Cheb Basin. We used the data from the 2008 earthquake swarm located in the NK focal zone (Horálek et al., 2009; Fischer et al., 2010) (see Figure 1). The waveforms recorded at 22 WEBNET network stations were cross correlated for the *P* waves, rotated, aligned, and stacked following the approach of Hrubcová et al. (2013). This enabled to extract the reflected *SmS* phases in the *S* wave coda. These phases were inverted for laterally varying Moho depth by the ray tracing and a grid search inversion algorithm. Because of high-frequency content of the waveforms, the interpretation of the *SmS* phases from local seismicity provided a high-resolution image of the lower crust. In this interpretation, the crust was assumed to be isotropic; effects of crustal anisotropy detected in the crust (Vavryčuk, 1993; Vavryčuk et al., 2004) should not affect the results as discussed by Hrubcová et al. (2013).

The waveform cross correlation of the direct *P* waves enabled to detect precise onsets of the *SmS* phases in the waveforms. The *P* onsets were utilized for a primary waveform alignment and then associated with the traveltimes calculated by ray tracing. In order to remove effects of a local structure beneath each station, the traveltimes of the Moho reflected phases were calculated relative to the direct *P* waves. These traveltimes served for subsequent alignment of traces to enhance a visibility of the Moho phases in the seismograms. The waveforms aligned according to the *SmS* phases were stacked and inverted for the Moho depth with a grid search algorithm. The data were processed for each station separately to evaluate lateral variations in the depth of the crust/mantle boundary. The accuracy of the depth determination of the crust/mantle boundary is on the order of 0.25 km. Details of processing with synthetic and resolution tests are discussed in Hrubcová et al. (2013).

The *SmS* phases are reasonably pronounced and well separated from the direct *S* wave onsets at all WEBNET stations; their inversion indicates both a reflective zone at the lower crustal depths and a single interface with a sharp velocity contrast. Figure 5 shows the waveforms recorded at station KOPD of the WEBNET network. Since there is a good spatial correlation of the 2008 earthquake swarm (see NK focal zone in Figure 1) with termination of the reflectivity, we check for details in lower crustal features. For this reason, the data set is

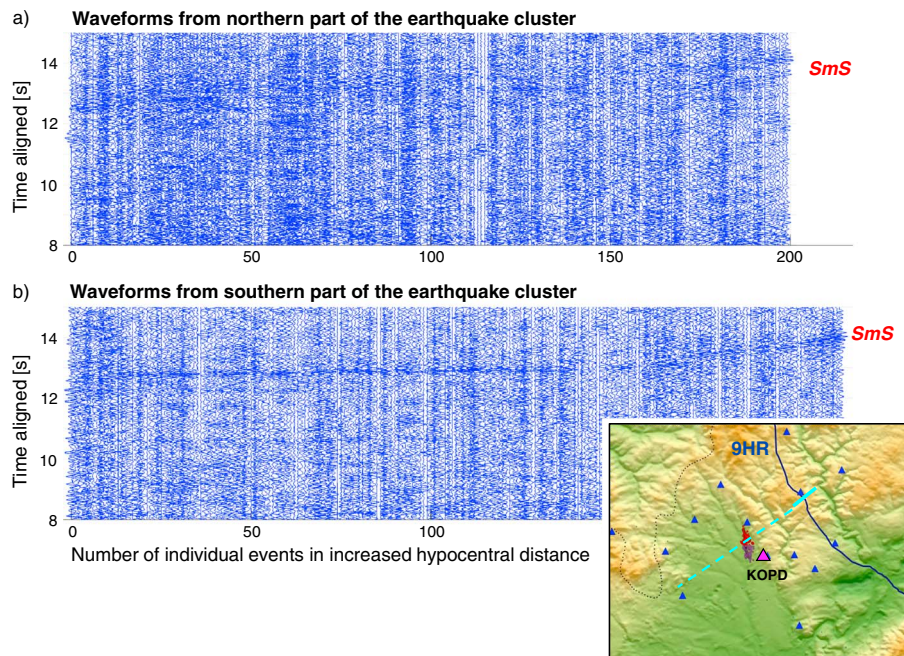


Figure 5. The reflected *SmS* phases in the waveforms of local earthquakes that occurred at the NK focal zone and were recorded at the station KOPD (pink triangle) of the WEBNET network (blue triangles). (a) Waveforms of earthquakes from the northern part of the 2008 swarm cluster (red dots in the inset) exhibit less pronounced *SmS* phases with more reflectivity indicating a transition zone in the northwest. (b) Waveforms of earthquakes from the southern part of the 2008 swarm cluster (violet dots in the inset) show a strong *SmS* phase indicating a single sharp interface in the southeast. Waveforms are aligned according to the *P* wave arrivals with increasing hypocentral distance. The end of the reflective lower crust (blue line in the inset) coincides with the transition from thick to thin lower crust detected along 9HR profile.

divided into two parts: the northern and the southern clusters of the 2008 earthquake swarm to illustrate the abrupt termination of this reflectivity. Waveforms from the northern cluster exhibit widespread *SmS* phases indicating a broad zone of reflectivity in the north (Figure 5a); data from the southern cluster show strong *SmS* phases indicating a single sharp interface in the south (Figure 5b).

The thickness of the lower crustal layer inverted from the *SmS* phases is presented in Figure 6a. The thickness varies from 1 to 4 km within a depth range of 27–31.5 km and is delimited by the reflections from its top and bottom boundaries. It exhibits a thick lower crustal layer of 4 km northwest of the NK focal zone and a thin layer in the southeast with thickness of only 1–1.5 km. The change of a broad reflective zone to a strong-contrast interface is abrupt and trends in the NE-SW direction in a prolongation of the northern Eger Rift shoulder. Figure 6b shows a good spatial correlation of the 2008 earthquake swarm with termination of the lower crustal reflectivity detected along the 9HR profile.

The interpretation of the *SmS* phases gives detailed and focused information on the crust/mantle transition aside from the 9HR profile. It delineates the termination of the broad reflective zone and its change into a strong-contrast interface. Its position is also in agreement with the surface manifestation of dextral shear fault zone Nová Ves of the same direction recognized by Bankwitz, Bankwitz, et al. (2003) at the northern edge of the Cheb Basin (see Figure 6a). Thus, the termination of reflectivity can be seen as a robust structural phenomenon manifested by several features at different crustal levels: (1) by the dextral shear zone detected by Bankwitz, Bankwitz, et al. (2003), (2) by swarm seismicity at ~10 km depth, and (3) by the termination of reflectivity and change into the strong-contrast interface at the lower crust.

4. Magmatic Underplating

Magmatic underplating occurs when basaltic magma is trapped during its rise to the surface at the crust/mantle boundary. This process is possible due to reduced density contrast (buoyancy) between the rising magma and the surrounding rocks. When magma cools, it results in thickening of the lower crust. Ancient underplated material is characterized by high seismic velocities (*P* waves in the range of

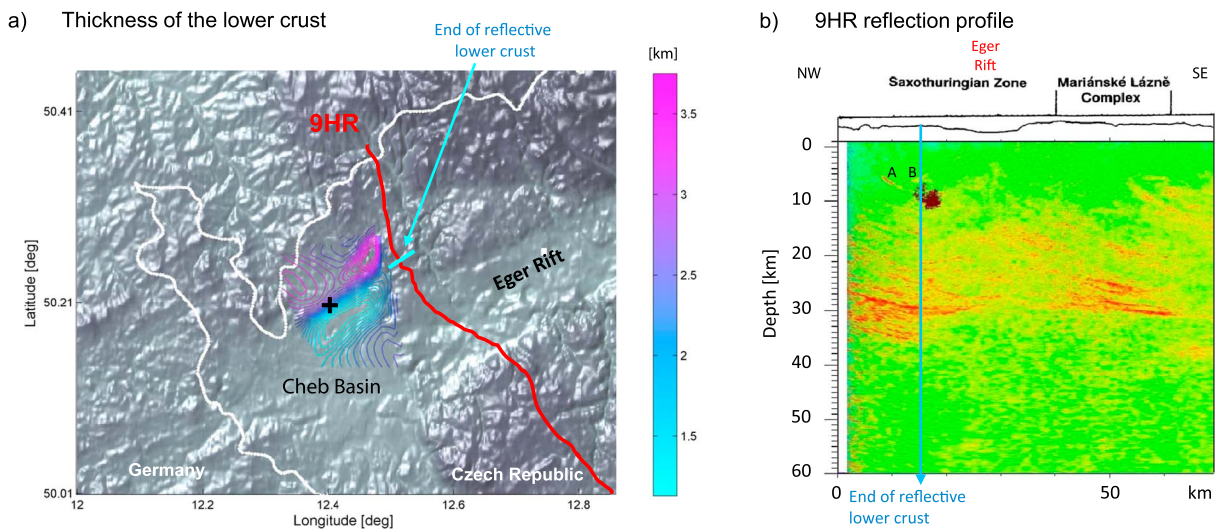


Figure 6. (a) Thickness of the lower crustal zone from the interpretation of the *SmS* phases detected in the local seismicity projected at the topography map. Thickness variation is shown by the color scale at the right. Note the abrupt change of a thick lower crust in the northwest to a strong-contrast interface in the southeast trending in the NE-SW direction in a prolongation of the northern Eger Rift shoulder. The red line shows the position of the 9HR profile; the black cross marks the quarry with a detected dextral shear fault zone at the surface (after Bankwitz, Bankwitz, et al., 2003). (b) Reflection profile 9HR (after Mullick et al., 2015) with the projection of swarm earthquakes in the main NK focal zone (brown dots at ~10 km depth) above the termination of the lower crustal reflectivity. A and B, distinct reflectors forming the V-shape bright spot in the upper crust. Note the abrupt termination of seismic reflectivity at a distance of 14 km at the 9HR profile coinciding with the transition from a broad zone to a strong-contrast interface at the lower crust detected in the interpretation of local seismicity.

6.9–7.8 km s^{−1}) and increased densities in comparison to normal (i.e., more felsic) crustal lithologies. Its upper and lower boundaries are usually delimited by pronounced seismic reflectors despite relatively weak velocity contrasts. Occasionally, the underplated material can show an increased seismic reflectivity within the high-velocity layer (Thybo & Artemieva, 2013). If seismic reflectivity exists, it can be explained by the presence of elongated “thin” mafic bodies (generally 300–500 m thick and ~400 km long), which may be interpreted as sill-like intrusions or dykes into the preexisting less mafic continental lower crust. On the other hand, massive magma chamber cooling or repeated intrusions into the mafic lower crust with strong magmatic overprinting may result in reflection-free bodies (Thybo & Artemieva, 2013). The wide area of the Cheb Basin in the western Eger Rift exhibits a high-velocity lower crust with both high reflectivity (lamination) and reflection-free lower crustal zones, which can be related to magmatic underplating. Based on the character of the seismic lower crustal image, we can distinguish two different underplating stages related to the Late Paleozoic and Cenozoic magmatism.

4.1. Paleozoic Magmatic Underplating

West of the Eger Rift, the lower crustal layer shows a high-velocity gradient, strong reflections from its top, and an increased reflectivity masking weak Moho reflections at its bottom. This is documented by seismic data of CEL09 (Hrubcová et al., 2005; Hrubcová & Geissler, 2009), GRANU'95 (Enderle et al., 1998), and MVE 90 (DEKORP Research Group, 1994) profiles. Such a highly reflective lower crust seems to be characteristic for the Saxothuringian unit and is generally related to the Variscan orogeny (Enderle et al., 1998). The Variscan tectonics and the pre-Eger Rift origin can further be denoted by the inclination of the reflection bands toward the southeast, representing the underthrusting of the Saxothuringian under the Moldanubian and Teplá-Barrandian (McCann, 2008) as visible at distances of 0–13 km along the 9HR profile (see Figure 4).

A reflective lower crust is a phenomenon frequently observed in Caledonian and Variscan areas, and the most common explanations assume the presence of densely spaced thin layers of high and low velocities. This can be represented, for example, by alternating mafic/ultramafic material. The reflective zone can also be attributed to subhorizontal lamina of dense mafic rocks or melt within felsic granulites or garnet pyroxene granulites (Handy & Streit, 1999; Morozov et al., 2001). In addition, the lower crustal reflectivity can be affected by solidified intrusions most probably of amphibolite-rich composition, possibly stretched and arranged horizontally. A noritic xenolith showing weak layering of the main components represent a sample from

solidified intrusion from the lower crust (Geissler et al., 2007). To conclude, the high-velocity reflective lower crust west of the Eger Rift can be related to the magmatic episode of the Late Variscan age.

4.2. Late Cenozoic to Recent Magmatic Underplating

In the Cheb Basin, the lower crust exhibits an abrupt termination of its reflectivity. A strong reflector at the top of the lower crust at depths of ~28–30 km (after Mullick et al., 2015) (see Figure 4) can be traced at distances of 14–75 km along the 9HR profile. It is also in agreement with a strong reflector at the top of high-velocity lower crust interpreted by Hrubcová et al. (2005) along the CEL09 profile. Together with velocities of 6.9–7.5 km s⁻¹ (Hrubcová et al., 2005), it forms a high-velocity reflection-free body. Deeper reflectors at distances between 45 km and 75 km at depths of ~38–41 km along the 9HR profile are also in agreement with the results of Hrubcová et al. (2005) and mark its bottom delimitation as a transition from the crust to the mantle. Consistently with these results, the abrupt change of the lower crustal reflectivity is documented in data from local seismicity (Figure 5). These data show a strong reflector and absence of reflectivity toward the southeast in a prolongation of the northern shoulder of the Eger Rift (Figure 6). Above, such termination of the lower crust reflectivity can be traced up to the surface where it is mapped by a shear fault zone detected by Bankwitz, Bankwitz, et al. (2003).

The extent of the lower crustal body indicated by seismic data correlates roughly with the occurrence of mantle-derived fluid emanations at the surface (Figure 4). The degassing centers CB and ML (Figure 2) show a high gas flow of nearly pure CO₂ (CO₂ content >99 vol %); the δ¹³C values close to the MORB range and high mantle-derived helium fractions point to the lithospheric mantle origin of the fluids (e.g., Bräuer et al., 2008) (Table 1). Present geodynamic activity, manifested by large gas flow and progressive increase of mantle-derived helium at degassing locations in the Cheb Basin, thus indicates the ongoing magmatic activity beneath this area (Bräuer et al., 2005, 2009; Kämpf et al., 2013).

Mantle xenolith studies (Geissler et al., 2007) provided evidence of a magma source between the uppermost mantle and the lower crust. The Quaternary volcanoclastic rocks of the Mýtina Maar (MM) at the Tachov Fault (age 0.29 Ma; Mrlina et al., 2007), deposited at the outer rim of the maar, contain xenoliths from uppermost part of the lithospheric mantle. They are represented by wehrlites and clinopyroxenites; some of them also contain a significant amount of amphibole. Also, megaxenocrysts are found (phlogopite, amphibole, clinopyroxene, and olivine). Most of the samples are cumulates of alkaline melts, fragments of pegmatitic veins, and rocks from metasomatic lithospheric upper mantle. According to Geissler et al. (2007), the geothermobarometry indicates depths of their origin at about 25 to 40 km. These rocks have lower seismic velocities than common upper mantle rocks and indicate a shallow lithospheric mantle (or the crust/mantle transition) strongly altered by magmatic processes. Seismic velocities of these rock samples (estimated from modal composition due to small sample size; Geissler et al., 2007) are in agreement with the values of 6.9–7.5 km s⁻¹ detected by Hrubcová et al. (2005) in the lower crust at the refraction profile CEL09. In deeper parts, at the crust/mantle transition at depths of 34–36 km, the velocities of 7.5 to 7.9 km s⁻¹ (Hrubcová et al., 2005) are still lower than common mantle velocities (>7.9 km s⁻¹) and can indicate the presence of up to 3–5% melt as discussed by Faul et al. (1994). Also, water-bearing minerals like phlogopite or amphibole detected in xenoliths can decrease seismic velocities in this area compared to the uppermost mantle as suggested by Glahn et al. (1992).

The estimated depths of origin of xenoliths and thus the stagnation level of rising magma are at ~25–40 km, which is in agreement with the depth extent of the lower crustal body detected from the 9HR reflection and CEL09 refraction profiles. Similarly, Brandl et al. (2015) investigated the composition of clinopyroxene phenocrysts from the Quaternary ZH volcano (Figure 1) and determined the thermobarometric conditions of crystallization at a depth range of ~20–40 km. Thus, the nonreflective lower crust in the western Eger Rift can be seen as a high-velocity ultramafic magmatic body related to the ongoing late Tertiary and Quaternary to present magmatic activity. This is in agreement with a regional distribution of calculated Moho temperatures with increased values of slightly over 600°C for the weakened zone of the Eger Rift and its northern rim, the Krušné Hory Mountains (Čermák et al., 1991). As a consequence, the surface heat flow of 66 mW m⁻² is also increased compared to the surrounding units (Förster & Förster, 2000).

The lateral extent of the high-velocity nonreflective lower crust related to the late Cenozoic magmatic body is shown in Figure 7. In the west and northwest, this reflection-free magmatic body is delimited by the

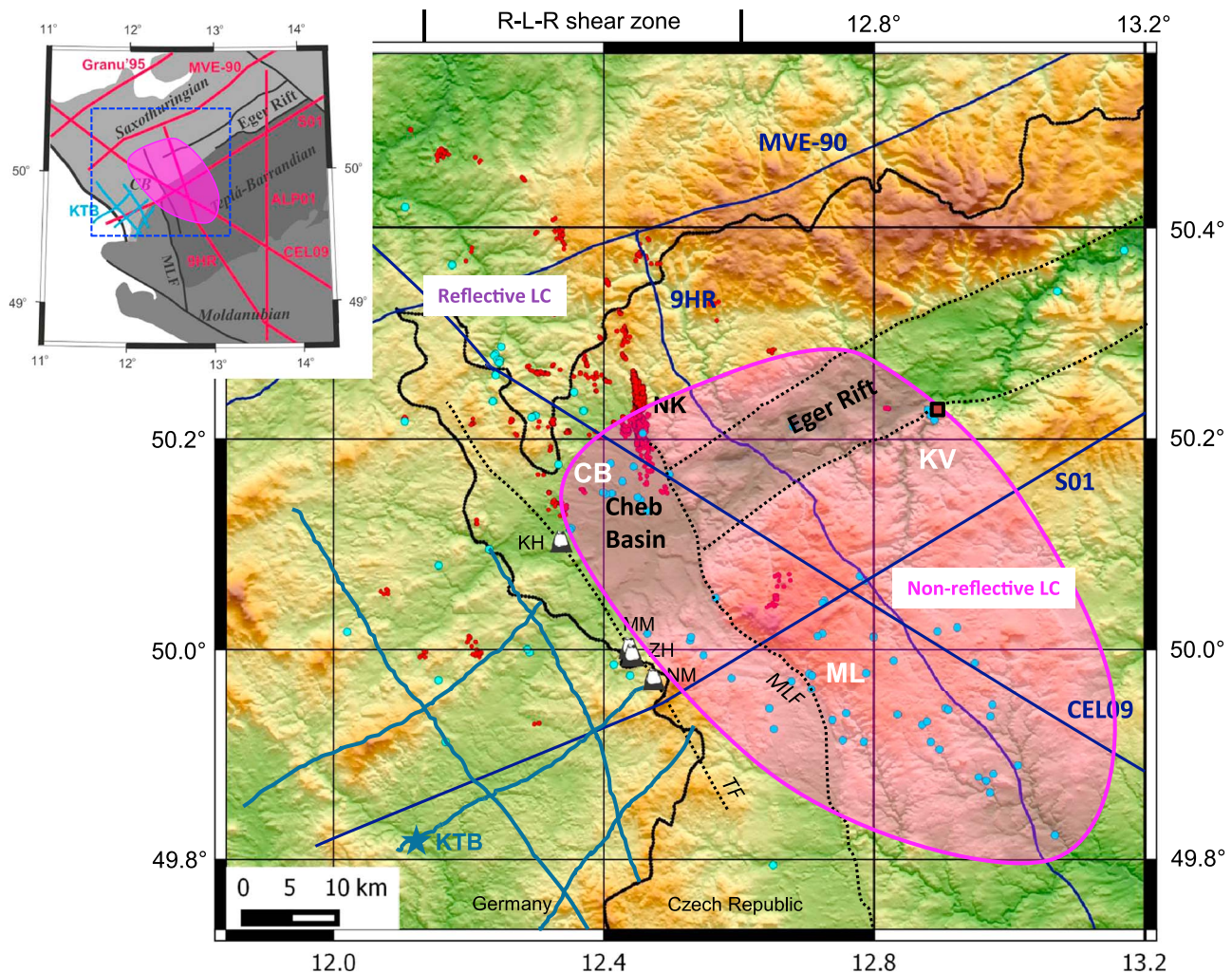


Figure 7. Lateral extent of the late Cenozoic magmatic body in the lower crust (pink) projected at the surface (indication according to seismic data, gas-geochemistry, and volcanic activity). Degassing centers CB, ML, and KV are indicated. Epicenters of local swarm earthquakes in the period of 1995–2015 (double difference locations located by Hypo-DD; Bouchaala et al., 2013) are marked by the red dots; the light blue dots represent fluid emanations at the surface. Seismic refraction/reflection profiles are marked by the blue lines. Four Quaternary volcanoes are indicated by the black/white cones. The brown rectangle represents the occurrence of the hydrothermal travertine in the KV degassing center. MLF, Mariánské Lázně Fault; TF, Tachov Fault. The inset shows the late Cenozoic magmatic body in the lower crust projected at a superposition of the main tectonic units in West Bohemia.

termination of the lower crustal reflectivity documented at a distance of 14 km along the 9HR profile. It coincides with the area of the lower crustal thinning mapped from *SmS* reflected phases in the western edge of the Cheb Basin. In the southwest, it may be traced close to the NW-SE striking Tachov Fault Zone, the tectonic line with an exposition of recent Quaternary volcanic activity. This fault may indicate a termination of the lower crustal reflectivity detected at the KTB seismic reflection profiles (DEKORP Research Group, 1988). The increased lower crustal reflectivity mapped along these profiles to the southwest could represent a mixture of old Variscan structure and younger sill intrusions as discussed by Trappe and Wever (1990). The southeastern extent of the magmatic body is delimited by the termination of the reflection-free lower crust at a distance of 75 km along the 9HR profile and the termination of high-velocity lower crust at a distance of 150 km along the CEL09 profile. This coincides with the occurrence of the degassing center ML and its periphery. Its northern and northeastern extents can be delineated by the magmatic activity responsible for the formation of the travertine (Vylita et al., 2007) and surface emanations of mantle-derived CO₂-rich fluids in the KV degassing center. The refraction profile S01 shows a change in the character of the lower crust (see Grad et al., 2008) close to the KV center, which may be connected with the delimitation of the magma body in the northeast (see Figure 7).

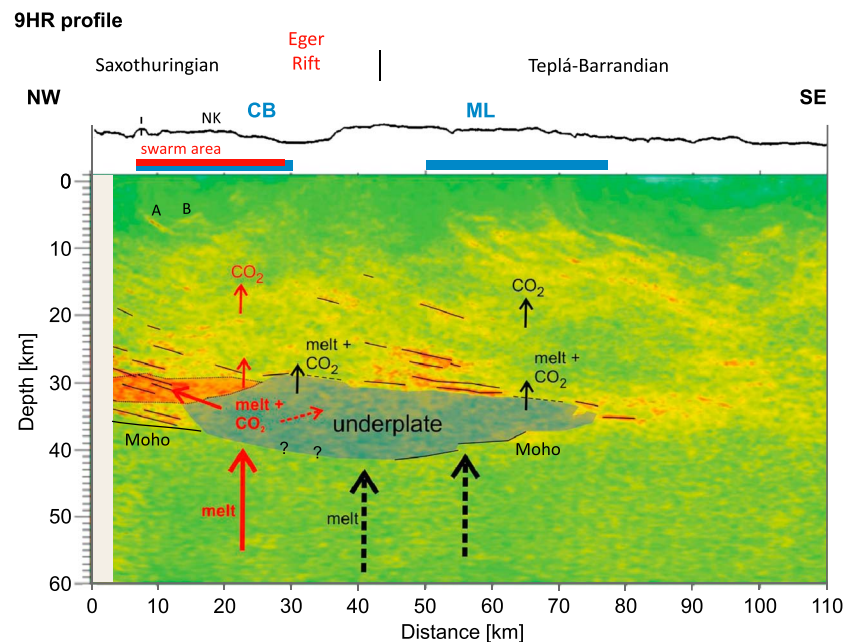


Figure 8. The interpreted cross section showing a spatial distribution of the late Cenozoic magmatic underplated body. The shape of the nonreflective lower crust and its transition to the surrounding reflective Variscan region are clearly delineated on the prestack image of the 9HR profile (Mullick et al., 2015). A and B, distinct reflectors forming the V-shape bright spot in the upper crust. The red arrows suggest possible paths for the active underplate magmatic activity, whereas the black solid and dashed arrows indicate the current (steady state) and past activities. Since different data sets are merged, the structure of the lower crust highlights relative differences and lateral changes; absolute depths depend on the velocity model adopted in the migration. The blue bars represent the extent of the CB and ML degassing centers at the surface; the red bar represents the extent of seismicity projected at the surface. NK, the Nový Kostel focal zone.

5. Discussion

5.1. Two Types of Lower Crust

The interpretation of both types of the lower crust in the western Eger Rift is summarized in Figure 8, which shows a schematic cross section based on a prestack reflection image of the 9HR profile. The figure depicts a presumed extent of the late Cenozoic magmatic underplated body as well as its delimitation from a surrounding laminated Variscan lower crust with the indication of a recent activity and presumed activity in the past. Since different data sets are merged, the interpretations may not reflect actual depths of the lower crustal structures. Instead, they focus on lateral changes in physical properties (e.g., reflectivity and mantle-derived helium fractions). The uncertainties in the depth determination are ± 2 km depending on the velocity model used in the migration process.

The two types of the lower crust in the Cheb Basin evidencing two different episodes may not be limited to the lower crust only. Several other investigations point to a whole-crustal extent of this feature. The abrupt termination of the lower crustal reflectivity coincides at the surface with the dextral shear fault zone recognized by Bankwitz, Bankwitz, et al. (2003). In the upper crust, the V-shaped bright spot detected along the 9HR profile (Mullick et al., 2015) is located in the same place. The same V-shape interface at depths of 3.5–6 km is also identified when interpreting waveforms from local seismicity by Hrubcová et al. (2016). A midcrustal reflector at depths of 18 and 20 km along the CEL09 profile is disrupted in the area of the Cheb Basin (Hrubcová et al., 2005). The high-velocity upper crustal body interpreted along the S01 refraction profile of the Sudetes 2003 experiment (Grad et al., 2008) is disconnected in the area of the Cheb Basin and the ML Fault. The occurrence of seismicity at ~ 10 km depth is explained by reactivation of previously ruptured deep-seated fault segments (Bankwitz, Schneider, et al., 2003; Fischer et al., 2014; Vavryčuk et al., 2013). At deeper levels, Babuška and Plomerová (2008) assume a contact of three lithospheric domains forming a triple junction in the Cheb Basin. In this respect, lower amplitudes of reflections from the top of the lower crust visible along the 9HR profile beneath the Eger Rift (distance of 29–35 km; see Figures 4 and 8) might be connected with the same whole-crustal structure, although Tomek et al. (1997) explained their origin by technical difficulties of the 9HR data acquisition.

5.2. Origin of Reflection-Free Magma Body

The structure resulting from underplating processes may, in general, take many forms comprising both reflective and nonreflective lower crust. In young rift zones, a combination of both is observed, for example, in the Baikal Rift where the underplated material at the base of the crust is supposed to be in the form of mafic sills directly below the graben (Thybo & Nielsen, 2009). A strong wide-angle seismic reflectivity is observed in a 50–80 km wide zone, whereas a high-velocity transparent lower crust is detected outside this zone with properties resembling the adjacent Siberian Craton. A similar setting is detected in the southern Kenya Rift Zone with a reflective high-velocity lower crustal body directly below the graben and nonreflective lower crust outside (Birt et al., 1997). On the contrary, a nonreflective magmatic body at the base of the crust was identified in the Oslo Graben in Norway with transparent underplated body indicating long-term cooling of a large magma chamber (Stratford & Thybo, 2011). An underplated zone of the crust at the North Atlantic margins shows a high-velocity zone as seismically reflective, whereas the main underplated body is reflection-free. This indicates the underplated layer as sill intrusions into a preexisting lower crust during rifting with a substantial volume of magma supplied at time of breakup followed by a long-lasting solidification of the magmatic body (White et al., 2008).

In the Cheb Basin, the origin of the reflection-free body may result from massive magma chamber cooling or repeated intrusions with magmatic overprinting of an already mafic Variscan lower crust as suggested in scenario by Thybo and Artemieva (2013). In their concept, the late Cenozoic to Quaternary magmatic underplating in the Cheb Basin resembles models of crustal stretching leading to massive mafic intrusion/underplating in the form of a crustal batholith or layered intrusion/underplate along the Moho possibly at later stages of the development (Thybo & Artemieva, 2013; their Figure 13, models b1 and b2).

5.3. Recent Magmatic Activity

The geophysical imaging provides detailed structural information; however, it does not indicate how and when the processes took place. This can be documented by isotope time series studies, which give evidence on still active processes. In the western Eger Rift area, the emanating fluids show high mantle-derived helium fractions with the $^3\text{He}/^4\text{He}$ ratios ranging between 3.3 and 6.3 Ra at all sites of the degassing centers CB and ML (Figure 2). Though the gas flow and $\delta^{13}\text{C}$ values are in the same order of magnitude, the degassing centers display differences. Compared to the ML in the southeast, the CB center exhibits an increase of mantle-derived fractions over the last 25 years of monitoring. The highest $^3\text{He}/^4\text{He}$ ratios were recorded at mofettes at the eastern flank of the Cheb Basin along the PPZ (Figure 2; nos. 23 and 24) and nearby (nos. 22 and 91) (Bräuer et al., 2008, 2009, 2011). Their values are close to the helium isotope range of the European subcontinental mantle (ESCM) (Gautheron et al., 2005). Clear fractions of the mantle-derived helium were also recorded at mofettes in the southwest (Františkovy Lázně and Soos; nos. 110 and 26). A temporal (limited in time) increase of the $^3\text{He}/^4\text{He}$ ratios (>6 Ra) recorded before the earthquake swarms 2000 (Bräuer et al., 2008) and 2008 (Bräuer et al., 2014) in the eastern part of the Cheb Basin might be another indication for an active deep-seated magmatic process.

In addition, the increase of the mantle-derived helium correlates with the intensity of seismicity. The Cheb Basin and especially the NK focal zone show a pronounced seismic activity of local earthquakes at a midcrustal level, whereas the seismicity is low in the ML center. The progressive temporal increase in mantle-derived helium fractions may indicate a connection of faults with the deeper parts of the crust (Bräuer et al., 2011). Further, current seismicity, commonly discussed as triggered by fluid activity (e.g., Fischer et al., 2014; Vavryčuk & Hrubcová, 2017), also points to deep-seated faults serving as paths for intrusion of fluids. These faults might be connected with the Cenozoic reactivation of deep NE-SW and NW-SE oriented faults as the elements of the N-S striking trans-lithospheric Regensburg-Leipzig-Rostock Zone allowing rapid ascent of melilitites, basanites, alkali basalts, ultramafic lamprophyres, and carbonatites (Brandl et al., 2015; Geissler et al., 2007; Ulrych et al., 2016). In this way, the Cheb Basin can be perceived as one of the most active regions in Central Europe and as an indicator of today's magmatic activity.

The beginning and early evolution of the recent magmatic underplate is not clear. According to Ulrych et al. (2011, 2013) the volcanic activity was present in the Slavkovský Les/Cheb-Domažlice Graben in the middle and upper Miocene. This area coincides with the observed high-velocity lower crust with reflection-free body. The volcanic rocks show a bimodal distribution (nephelinite/basanites and tephrites/phonolites), where the

latter implies that the magmas deeper in the lithosphere can evolve through a differentiation and partial crystallization. The uplift of the Eger Rift shoulders Krušné Hory and Slavkovský Les block Mountains (Andreani et al., 2014) (see Figure 1) is another indication of geodynamic activation in the middle and upper Miocene. However, it is not clear if this middle to late Miocene geodynamic activity between ~17 Ma to ~4.7 Ma is connected with the most recent activity because of a gap till ~0.3 Ma. Since then, we have evidence of volcanic activity along the Tachov Fault Zone from MM and NM (Mrlina et al., 2007, 2009; Rohrmüller et al., 2017) as well as from hydrothermal activity in the KV center with travertine deposits dated back to 0.23 Ma (Vylita et al., 2007).

6. Conclusions

We interpreted seismic, seismological, petrological, and gas-geochemical observations in the western Eger Rift, which point to a local-scale magmatic emplacement at the base of the continental crust within a new rift environment. The concept of magmatic underplating is evidenced by detecting two types of the lower crust: (1) a high-velocity lower crust with a pronounced reflectivity and (2) a high-velocity reflection-free lower crust. The character of the underplated material enables to differentiate timing and tectonic setting of the two episodes with different times of origin.

1. The underplating related to the Late Variscan age is evidenced by a high P wave velocity lower crust ($6.9\text{--}7.5\text{ km s}^{-1}$) at the CEL09 refraction profile. It is complemented by a lower crustal reflectivity up to a distance of 14 km along the 9HR profile and by analysis of local seismicity. Such a lamination is characteristic for the Saxothuringian unit in the west and northwest of the Eger Rift.
2. The high-velocity reflection-free lower crustal body detected at a distance of 14–75 km along the 9HR profile together with a strong reflector at its top at depths of ~28–30 km (also evidenced from the receiver functions) indicates magmatic underplating of the late Cenozoic to recent. Deeper reflectors at distances of 45 km and 75 km at depths of ~38–41 km along the 9HR profile (see also Tomek et al., 1997) mark its bottom delimitation as a transition from the crust to the mantle. It agrees with the high-velocity lower crust terminating at a distance of 150 km along the CEL09 profile (Hrubcová et al., 2005). In the southwest, the high-velocity body might be traced close to the NW-SE striking Tachov Fault, the tectonic line with the exposition of recent Quaternary volcanic activity, where the termination of the lower crustal reflectivity is suggested from the KTB seismic reflection profiles (DEKORP Research Group, 1988). In the northeast, it is delimited by the hydrothermal activity in the KV degassing center and by a lateral change in the lower crust along the S01 profile (Grad et al., 2008).
3. The reflection-free magmatic body in the lower crust correlates with the occurrence of the mantle-derived fluid emanations at the surface. A large gas flow and a clear increase of mantle-derived helium fractions point to the actively degassing magma in the upper mantle (Bräuer et al., 2009; Kämpf et al., 2013).
4. The strong seismic reflectivity attributed to the Variscan lower crust may represent the intrusions in the form of sill-like features, whereas the reflection-free body attributed to the late Cenozoic lower crust may result from a massive magma-chamber cooling as discussed by Thybo and Artemieva (2013). The contact of the reflective and nonreflective crust can show a mixture of an old Variscan structure and new sill intrusions. Patchy reflections within parallel orientated high reflectivity of the Variscan origin might indicate minor intrusions within the still intact lower crust.
5. The composition of xenoliths of 0.29 Ma old volcanics documents the origin depths of the magma at ~25–40 km, which corresponds to the high-velocity lower crust. This depth range represents the intrusion/stagnation level of the uprising magma. According to Geissler et al. (2007), the upper mantle and lower crust xenoliths show significant amount of amphibole, which increases the seismic velocities of the lower crust and decreases the upper mantle velocities of the surrounding upper mantle rocks. Resulting seismic velocities are in agreement with the modeled seismic velocities in the lower crustal layer of $6.9\text{--}7.5\text{ km s}^{-1}$ (Hrubcová et al., 2005).
6. The helium isotope ratios in emanating fluids point to their origin from the upper mantle. The highest recorded helium isotope ratios in the fluids are in agreement with those measured in ultramafic xenoliths from other European volcanic provinces ($6.32 \pm 0.39\text{ Ra}$; Gautheron et al., 2005) documenting a strong magmatic ESCM component. The distribution of mantle-derived fluid emanations at the surface correlates with the position and extent of the magma body in the lower crust.

7. The high helium isotope ratios evince a recent magmatic origin. A different behavior of fluids in the CB degassing center with the highest $^3\text{He}/^4\text{He}$ values of 6.3 Ra compared to the KV and ML centers, the recent seismic activity, and the Quaternary volcanic system along the Tachov Fault at the southwestern flank of the Cheb Basin point to the ongoing magmatic activity below this area. These phenomena are connected with the present activity within the broad late Cenozoic magmatic body and its reactivation during the Quaternary (in the last 0.3 Ma from mid-Pleistocene to Holocene). This is also supported by the hydrothermal activity of the travertine in the KV degassing center dated 0.23–0 Ma.

Although the age of the nonreflective magma body is difficult to constrain precisely, the late Cenozoic/Quaternary volcanism and the present geodynamic activity indicate that it is probably not older than 0.3 Ma. This suggests that the magmatism beneath the western Eger Rift is an ongoing process and represents active magmatic underplating in the continental lithosphere. In a broader sense, it provides important insight into the magmatic accretionary processes in the continental crust and has a high potential for detection and evaluation of a deep magmatic/fluid activity within young and new continental rift areas.

Despite the evidence of ongoing processes, there are still questions that remain open. One of them is connected with the source of the magma in the lithospheric mantle. A possible origin of the magmatic material is discussed by Plomerová et al. (2016) based on a teleseismic tomography. They see low-velocity perturbations in the P , S , and PKP wave models at ~80–170 km depths. Instead of a baby plume, they accentuate an upward flow of a hot mantle material penetrating along boundaries of the mantle lithosphere domains from the sublithospheric mantle to the surface in the area of the triple junction. Another open question relates to the discrepancy between the amount of underplated material and the surface expression of volcanism. Finally, the beginning of the recent underplating episode remains unclear with no definite answer whether it started in the Miocene and represents a continuation of the Cenozoic (middle and upper Miocene) activity or reinitiated at about 0.3 Ma ago.

Acknowledgments

This research was supported by the Grant Agency of the Czech Republic, grants 17-19297S and 16-19751J and by the German Research Foundation, grant KA 902/16. It was also partially supported by the Slovak grant agency Vega, project 1/0141/15. Waveforms of the WEBNET network are accessible from IRIS fed-catalog data center (Institute of Geophysics, 1991). The authors would like to thank Siegfried Siegesmund for introduction to the magmatic underplating exposed at the surface in the Ivrea zone, Italy. The manuscript benefited from valuable comments by the Editor Cladio Faccenna, the Associate Editor Jeffrey Gu, and two anonymous reviewers.

References

- Andreani, L., Stanek, K. P., Gloaguen, R., Krentz, O., & Domínguez-González, L. (2014). DEM-based analysis of interactions between tectonics and landscapes in the Ore Mountains and Eger Rift (East Germany and NW Czech Republic). *Remote Sensing*, 6(9), 7971–8001. <https://doi.org/10.3390/rs6097971>
- Babuška, V., & Plomerová, J. (2008). Control of paths of quaternary volcanic products in western Bohemian Massif by rejuvenated Variscan triple junction of ancient microplates. *Studia Geophysica et Geodaetica*, 52(4), 607–630. <https://doi.org/10.1007/s11200-008-0040-0>
- Bankwitz, P., Bankwitz, E., Bräuer, K., Kämpf, H., & Störr, M. (2003). Deformation structures in Plio- and Pleistocene sediments (NW Bohemia, Central Europe). In P. Van Rensbergen, et al. (Eds.), *Subsurface sediment mobilization. Geological Society of London, Special Publication*, 216(1), 73–93. <https://doi.org/10.1144/GSL.SP.2003.216.01.06>
- Bankwitz, P., Schneider, G., Kämpf, H., & Bankwitz, E. (2003). Structural characteristics of epicentral areas in Central Europe: Study case Cheb Basin (Czech Republic). *Journal of Geodynamics*, 35(1–2), 5–32. [https://doi.org/10.1016/S0264-3707\(02\)00051-0](https://doi.org/10.1016/S0264-3707(02)00051-0)
- Birt, C. S., Maguire, P. K. H., Khan, M. A., Thybo, H., Keller, G. R., & Patel, J. (1997). The influence of pre-existing structures on the evolution of the southern Kenya Rift valley; evidence from seismic and gravity studies. *Tectonophysics*, 278(1–4), 211–242. [https://doi.org/10.1016/S0040-1951\(97\)00105-4](https://doi.org/10.1016/S0040-1951(97)00105-4)
- Bouchaala, F., Vavryčuk, V., & Fischer, T. (2013). Accuracy of the master-event and double-difference locations: Synthetic tests and application to seismicity in West Bohemia, Czech Republic. *Journal of Seismology*, 17(3), 841–859. <https://doi.org/10.1007/s10950-013-9357-4>
- Brandl, P. A., Genske, F. S., Beier, C., Haase, K. M., Sprung, P., & Krumm, S. H. (2015). Magmatic evidence for carbonate metasomatism in the lithospheric mantle underneath the Ohře (Eger) Rift. *Journal of Petrology*, 56(9), 1743–1774. <https://doi.org/10.1093/petrology/egv052>
- Bräuer, K., Kämpf, H., Koch, U., & Strauch, G. (2011). Monthly monitoring of gas and isotope compositions in the free gas phase at degassing locations close to the Nový Kostel focal zone in the western Eger Rift, Czech Republic. *Chemical Geology*, 290(3–4), 163–176. <https://doi.org/10.1016/j.chemgeo.2011.09.012>
- Bräuer, K., Kämpf, H., Niedermann, S., & Strauch, G. (2005). Evidence for ascending upper mantle-derived melt beneath the Cheb basin, central Europe. *Geophysical Research Letters*, 32, L08303. <https://doi.org/10.1029/2004GL022205>
- Bräuer, K., Kämpf, H., Niedermann, S., Strauch, G., & Tesař, J. (2008). The natural laboratory NW Bohemia—Comprehensive fluid studies between 1992 and 2005 used to trace geodynamic processes. *Geochemistry, Geophysics, Geosystems*, 9, Q04018. <https://doi.org/10.1029/2007GC001921>
- Bräuer, K., Kämpf, H., & Strauch, G. (2009). Earthquake swarms in non-volcanic regions: What fluids have to say. *Geophysical Research Letters*, 36, L17309. <https://doi.org/10.1029/2009GL039615>
- Bräuer, K., Kämpf, H., & Strauch, G. (2014). Seismically triggered anomalies in the isotope signatures of mantle-derived gases detected at degassing sites along two neighboring faults in NW Bohemia, Central Europe. *Journal of Geophysical Research: Solid Earth*, 119, 5613–5632. <https://doi.org/10.1002/2014JB011044>
- Brückl, E., Bleibinhaus, F., Gosar, A., Grad, M., Guterch, M., Hrubcová, P., ... Thybo, H. (2007). Crustal structure due to collisional and escape tectonics in the Eastern Alps region based on profiles Alp01 and Alp02 from the ALP 2002 seismic experiment. *Journal of Geophysical Research*, 112, B06308. <https://doi.org/10.1029/2006JB004687>
- Čermák, V., Král, M., Krešl, M., Kubík, J., & Šafanda, J. (1991). Heat flow, regional geophysics and lithosphere structure in Czechoslovakia and adjacent part of Central Europe. In V. Čermák & L. Rybach (Eds.), *Heat flow and the lithosphere structure* (pp. 133–165). Berlin: Springer. https://doi.org/10.1007/978-3-642-75582-8_6

- Christensen, N. I. (1996). Poisson's ratio and crustal seismology. *Journal of Geophysical Research*, 101(B2), 3139–3156. <https://doi.org/10.1029/95JB03446>
- DEKORP Research Group (1988). Results of the DEKORP 4/KTb Oberpfalz deep seismic investigations. *Journal of Geophysics*, 62, 69–101.
- DEKORP Research Group (1994). The deep reflection seismic profiles DEKORP 3/MVE-90. *Zeitschrift für Geologische Wissenschaften*, 22(6), 623–824.
- Enderle, U., Schuster, K., Prodehl, C., Schultze, A., & Briebach, J. (1998). The refraction seismic experiment GRANU'95 in the Saxothuringian belt, southeastern Germany. *Geophysical Journal International*, 133(2), 245–259. <https://doi.org/10.1046/j.1365-246X.1998.00462.x>
- Faul, U. H., Toomey, D. R., & Waff, H. S. (1994). Intergranular basaltic melt is distributed in thin, elongated inclusions. *Geophysical Research Letters*, 21(1), 29–32. <https://doi.org/10.1029/93GL03051>
- Fischer, T., Horálek, J., Michálek, J., & Boušková, A. (2010). The 2008 West Bohemia earthquake swarm in the light of the WEBNET network. *Journal of Seismology*, 14, 665–682.
- Fischer, T., Horálek, J., Hrubcová, P., Vavryčuk, V., Bräuer, K., & Kämpf, H. (2014). Intra-continental earthquake swarms in West-Bohemia and Vogtland: A review. *Tectonophysics*, 611, 1–27. <https://doi.org/10.1016/j.tecto.2013.11.001>
- Flechsig, C., Heinicke, J., Mrlina, J., Kämpf, H., Nickschick, T., Schmidt, A., ... Seidl, M. (2015). Integrated geophysical and geological methods to investigate the inner and outer structures of the Quaternary Mýtina maar (W-Bohemia, Czech Republic). *International Journal of Earth Sciences (Geol Rundsch)*, 104(8), 2087–2105. <https://doi.org/10.1007/s00531-014-1136-0>
- Förster, A., & Förster, H.-J. (2000). Crustal composition and mantle heat flow: Implications from surface heat flow and radiogenic heat production in the Variscan Erzgebirge (Germany). *Journal of Geophysical Research*, 105(B12), 27,917–27,938. <https://doi.org/10.1029/2000JB900279>
- Franke, W. (2000). The mid-European segment of the Variscides: Tectonostratigraphic units, terrane boundaries and plate tectonic evolution. In W. Franke, et al. (Eds.), *Orogenic processes: Quantification and modelling in the Variscan belt*. Geological Society of London, Special Publication, 179(1), 35–61. <https://doi.org/10.1144/GSL.SP.2000.179.01.05>
- Furlong, K. P., & Fountain, D. M. (1986). Continental crustal underplating—Thermal considerations and seismic-petrologic consequences. *Journal of Geophysical Research*, 91(B8), 8285–8294. <https://doi.org/10.1029/JB091iB08p08285>
- Gautheron, C., Moreira, M., & Allègre, C. (2005). He, Ne and Ar composition of the European lithospheric mantle. *Chemical Geology*, 217(1–2), 97–112. <https://doi.org/10.1016/j.chemgeo.2004.12.009>
- Geissler, W. H., Kämpf, H., Kind, R., Klinge, K., Plenefisch, T., Horálek, J., ... Nehybka, V. (2005). Seismic structure and location of a CO₂ source in the upper mantle of the western Eger rift, Central Europe. *Tectonics*, 24, TC5001. <https://doi.org/10.1029/2004TC001672>
- Geissler, W. H., Kämpf, H., Seifert, W., & Dulski, P. (2007). Petrological and seismic studies of the lithosphere in the earthquake swarm region Vogtland/NW Bohemia, central Europe. *Journal of Volcanology and Geothermal Research*, 159(1–3), 33–69. <https://doi.org/10.1016/j.jvolgeores.2006.06.011>
- Glahn, A., Sachs, P. M., & Achauer, U. (1992). A teleseismic and petrologic study of the crust and upper mantle beneath the geothermal anomaly Urach/SW-Germany. *Physics of the Earth and Planetary Interiors*, 69(3–4), 176–206. [https://doi.org/10.1016/0031-9201\(92\)90133-G](https://doi.org/10.1016/0031-9201(92)90133-G)
- Grad, M., Guterch, A., Mazur, S., Keller, G. R., Špičák, A., Hrubcová, P., & Geissler, W. H. (2008). Lithospheric structure of the Bohemian Massif and adjacent Variscan belt in central Europe based on profile S01 from the SUDETES 2003 experiment. *Journal of Geophysical Research*, 113, B10304. <https://doi.org/10.1029/2007JB005497>
- Handy, M. R., & Streit, J. E. (1999). Mechanics and mechanism of magmatic underplating: Inferences from mafic veins in deep crustal mylonite. *Earth and Planetary Science Letters*, 165(3–4), 271–286. [https://doi.org/10.1016/S0012-821X\(98\)00272-6](https://doi.org/10.1016/S0012-821X(98)00272-6)
- Heuer, B., Geissler, W. H., Kind, R., & Kämpf, H. (2006). Seismic evidence for asthenospheric updoming beneath the western Bohemian Massif, central Europe. *Geophysical Research Letters*, 33, L05311. <https://doi.org/10.1029/2005GL025158>
- Horálek, J., Fischer, T., Boušková, A., & Jedlička, P. (2000). The Western Bohemia/Vogtland Region in the light of the Webnet network. *Studia Geophysica et Geodaetica*, 44(2), 107–125. <https://doi.org/10.1023/A:1022198406514>
- Horálek, J., Fischer, T., Boušková, A., Michálek, J., & Hrubcová, P. (2009). The West Bohemian 2008-earthquake swarm: when, where, what size and data. *Studia Geophysica et Geodaetica*, 53, 351–358. <https://doi.org/10.1007/s11200-009-0024-8>
- Hrubcová, P., & Geissler, W. H. (2009). The crust-mantle transition and the Moho beneath the Vogtland/West Bohemian region in the light of different seismic methods. *Studia Geophysica et Geodaetica*, 53(3), 275–294. <https://doi.org/10.1007/s11200-009-0018-6>
- Hrubcová, P., Šroda, P., Špičák, A., Guterch, A., Grad, M., Keller, G. R., ... Thybo, H. (2005). Crustal and uppermost mantle structure of the Bohemian Massif based on CELEBRATION 2000 data. *Journal of Geophysical Research*, 110, B11305. <https://doi.org/10.1029/2004JB003080>
- Hrubcová, P., Vavryčuk, V., Boušková, A., & Bohnhoff, M. (2016). Shallow crustal discontinuities inferred from waveforms of microearthquakes: Method and application to KTB drill site and west bohemia swarm area. *Journal of Geophysical Research: Solid Earth*, 121, 881–902. <https://doi.org/10.1002/2015JB012548>
- Hrubcová, P., Vavryčuk, V., Boušková, A., & Horálek, J. (2013). Moho depth determination from waveforms of microearthquakes in the West Bohemia/Vogtland swarm area. *Journal of Geophysical Research: Solid Earth*, 118, 120–137. <https://doi.org/10.1029/2012JB009360>
- Institute of Geophysics, Academy of Sciences of the Czech Republic (1991). West Bohemia local seismic network. International Federation of Digital Seismograph Networks. Other/Seismic Network. <https://doi.org/10.7914/SN/WB>
- Jarchow, C. M., Thompson, G. A., Catchings, R. D., & Mooney, W. D. (1993). Seismic evidence for active magmatic underplating beneath the Basin and Range Province, western United States. *Journal of Geophysical Research*, 98(B12), 22,095–22,108. <https://doi.org/10.1029/93JB02021>
- Kämpf, H., Bräuer, K., Schumann, J., Hahne, K., & Strauch, G. (2013). CO₂ discharge in an active, non-volcanic continental rift area (Czech Republic): Characterization ($\delta^{13}\text{C}$, $^3\text{He}/^4\text{He}$) and quantification of diffuse and vent CO₂ emissions. *Chemical Geology*, 339, 71–83. <https://doi.org/10.1016/j.chemgeo.2012.08.005>
- Kopecký, L. (1978). Neoidic taphrogenic evolution and young alkaline volcanism of the Bohemian Massif. *Journal of the Geological Science (Geology)*, 31, 91–107.
- Málek, J., Horálek, J., & Janský, J. (2005). One-dimensional qP-wave velocity model of the upper crust for the West Bohemia/Vogtland earthquake swarm region. *Studia Geophysica et Geodaetica*, 49(4), 501–524. <https://doi.org/10.1007/s11200-005-0024-2>
- Marty, B., & Zimmermann, L. (1999). Volatiles (He, C, N, Ar) in mid-ocean ridge basalts: Assessment of shallow-level fractionation and characterization of source composition. *Geochimica et Cosmochimica Acta*, 63(21), 3619–3633. [https://doi.org/10.1016/S0016-7037\(99\)00169-6](https://doi.org/10.1016/S0016-7037(99)00169-6)
- Matte, P., Maluski, H., Rajlich, P., & Franke, W. (1990). Terrane boundaries in the Bohemian Massif: Result of large-scale Variscan shearing. *Tectonophysics*, 177(1–3), 151–170. [https://doi.org/10.1016/0040-1951\(90\)90279-H](https://doi.org/10.1016/0040-1951(90)90279-H)
- McCann, T. (Ed.) (2008). *The geology of Central Europe. Volume 1: Precambrian and Palaeozoic*. London: Geological Society.

- Mooney, W. D., Andrews, M. C., Ginzburg, A., Peters, D., & Hamilton, R. M. (1983). Crustal structure of the Northern Mississippi Embayment and a comparison of other continental rift zones. *Tectonophysics*, 94(1-4), 327–348. [https://doi.org/10.1016/0040-1951\(83\)90023-9](https://doi.org/10.1016/0040-1951(83)90023-9)
- Morozov, I. B., Smithson, S. B., Chen, J., & Hollister, L. S. (2001). Generation of new continental crust and terrane accretion in Southeastern Alaska and Western British Columbia: Constraints from P- and S-wave wide-angle seismic data (ACCRETE). *Tectonophysics*, 341(1-4), 49–67. [https://doi.org/10.1016/S0040-1951\(01\)00190-1](https://doi.org/10.1016/S0040-1951(01)00190-1)
- Mrlina, J., Kämpf, H., Geissler, W. H., & van den Bogaard, P. (2007). Proposed Quaternary maar structure at the Czech/German boundary between Mýtina and Neualbentreuth (western Eger Rift, Central Europe): Geophysical, petrochemical and geochronological indications. *Zeitschrift für Geologische Wissenschaften*, 35, 213–230.
- Mrlina, J., Kämpf, H., Kroner, C., Mingram, J., Stebich, M., Brauer, A., ... Seidl, M. (2009). Discovery of the first Quaternary maar in the Bohemian Massif, Central Europe, based on combined geophysical and geological surveys. *Journal of Volcanology and Geothermal Research*, 182(1-2), 97–112. <https://doi.org/10.1016/j.jvolgeores.2009.01.027>
- Mullick, N., Buske, S., Hrubcová, P., Růžek, B., Shapiro, S., Wigger, P., & Fischer, T. (2015). Seismic imaging of the geodynamic activity at the western Eger rift in central Europe. *Tectonophysics*, 647-648, 105–111. <https://doi.org/10.1016/j.tecto.2015.02.010>
- Plomerová, J., Munzarová, H., Vecsey, L., Kissling, E., Achauer, U., & Babuška, V. (2016). Cenozoic volcanism in the Bohemian Massif in the context of P- and S-velocity high-resolution teleseismic tomography of the upper mantle. *Geochemistry, Geophysics, Geosystems*, 17, 3326–3349. <https://doi.org/10.1002/2016GC006318>
- Prodehl, C., Mueller, S., & Haak, V. (1995). The European Cenozoic Rift System. In K. H. Olsen (Ed.), *Continental rifts: Evolution, Structure, Tectonics. Developments in Geotectonics* (Vol. 25, pp. 133–212). New York: Elsevier.
- Rohrmüller, J., Kämpf, H., Geiß, E., Großmann, J., Grun, I., Mingram, J., ... Nowaczyk, N. (2017). Reconnaissance study of an inferred Quaternary maar structure in the western part of the Bohemian Massif near Neualbenreuth, NE-Bavaria (Germany). *International Journal of Earth Sciences (Geol. Rundsch.)*. <https://doi.org/10.1007/s00531-017-1543-0>
- Rojík, P., Fejfar, O., Dašková, J., Kvaček, Z., Pešek, J., Sýkorová, I., & Teodoridis, V. (2014). Cheb Basin. In J. Pešek et al. (Eds.), *Tertiary basins and lignite deposits of the Czech Republic* (pp. 143–161). Prague: Czech Geological Survey.
- Stratford, W., & Thybo, H. (2011). Crustal structure and composition of the Oslo Graben, Norway. *Earth and Planetary Science Letters*, 304(3-4), 431–442. <https://doi.org/10.1016/j.epsl.2011.02.021>
- Thybo, H., & Artemieva, I. M. (2013). Moho and magmatic underplating in continental lithosphere. *Tectonophysics*, 609, 605–619. <https://doi.org/10.1016/j.tecto.2013.05.032>
- Thybo, H., & Nielsen, C. A. (2009). Magma-compensated crustal thinning in continental rift zones. *Nature*, 457(7231), 873–876. <https://doi.org/10.1038/nature07688>
- Tomek, Č., Dvořáková, V., & Vrána, S. (1997). Geological interpretation of the 9HR and 503M seismic profiles in Western Bohemia, in: Vrána, S., and Štědrá, V. (Eds.), *Geological model of Western Bohemia related to the KTB borehole in Germany. Journal of the Geological Science Geology*, 47, 43–50.
- Trappe, H., & Wever, T. (1990). Seismic evidence of increased tectonothermal activity near the Oberpfalz deep continental drilling location (SE Germany). *Geologische Rundschau*, 79(3), 649–658. <https://doi.org/10.1007/BF01879207>
- Ulrych, J., Ackerman, L., Balogh, K., Hegner, E., Jelínek, E., Pécskay, Z., & Foltýnová, R. (2013). Plio-Pleistocene basanitic and melilititic series of the Bohemian Massif: K-Ar ages, major/trace element and Sr-Nd isotopic data. *Chemie der Erde-Geochemistry*, 73(4), 429–450. <https://doi.org/10.1016/j.chemer.2013.02.001>
- Ulrych, J., Dostal, J., Adamovič, J., Jelínek, E., Špaček, P., Hegner, E., & Balogh, K. (2011). Recurrent Cenozoic volcanic activity in the Bohemian Massif (Czech Republic). *Lithos*, 123(1-4), 133–144. <https://doi.org/10.1016/j.lithos.2010.12.008>
- Ulrych, J., Krmíček, L., Tomek, Č., Lloyd, F. E., Ladenberger, A., Ackerman, L., & Balogh, K. (2016). Petrogenesis of Miocene alkaline volcanic suites from western Bohemia: Whole rock geochemistry and Sr-Nd-Pb isotopic signatures. *Chemie der Erde-Geochemistry*, 76(1), 77–93. <https://doi.org/10.1016/j.chemer.2015.11.003>
- Vavryčuk, V. (1993). Crustal anisotropy from local observations of shear-wave splitting in West Bohemia, Czech Republic. *Bulletin of the Seismological Society of America*, 83, 1420–1441.
- Vavryčuk, V., Bouchaala, F., & Fischer, T. (2013). High-resolution fault image from accurate locations and focal mechanisms of the 2008 swarm earthquakes in West Bohemia, Czech Republic. *Tectonophysics*, 590, 189–195. <https://doi.org/10.1016/j.tecto.2013.01.025>
- Vavryčuk, V., & Hrubcová, P. (2017). Seismological evidence of fault weakening due to erosion by fluids from observations of intraplate earthquake swarms. *Journal of Geophysical Research: Solid Earth*, 122, 3701–3718. <https://doi.org/10.1002/2017JB013958>
- Vavryčuk, V., Hrubcová, P., Brož, M., Málek, J., & ALP 2002 Working Group (2004). Azimuthal variation of Pg velocity in the Moldanubian, Czech Republic: Observations based on a multi-azimuthal common-shot experiment. *Tectonophysics*, 387(1-4), 189–203. <https://doi.org/10.1016/j.tecto.2004.06.015>
- Vylita, T., Žák, K., Čílek, V., Hercman, H., & Mikšíková, L. (2007). Evolution of hot-spring travertine accumulation in Karlovy Vary/Carlsbad (Czech Republic) and its significance for the evolution of Teplá valley and Ohře/Eger rift. *Zeitschrift für Geomorphologie*, 51(4), 427–442. <https://doi.org/10.1127/0372-8854/2007/0051-0427>
- Wagner, G. A., Gögen, K., Jonckheere, R., Wagner, I., & Woda, C. (2002). Dating of Quaternary volcanoes Komorná hůrka (Kammerbühl) and Železná hůrka (Eisenbühl), Czech Republic, by TL, ESR, alpha-recoil and fission track chronometry. *Zeitschrift für Geologische Wissenschaften*, 30, 191–200.
- Weinlich, F. H., Bräuer, K., Kämpf, H., Strauch, G., Tesářík, J., & Weise, S. M. (1999). An active subcontinental mantle volatile system in the western Eger rift, Central Europe: Gas flux, isotopic (He, C, and N) and compositional fingerprints. *Geochimica et Cosmochimica Acta*, 63(21), 3653–3671. [https://doi.org/10.1016/S0016-7037\(99\)00187-8](https://doi.org/10.1016/S0016-7037(99)00187-8)
- White, R. S., Smith, L. K., Roberts, A. W., Christie, P. A. F., & Kusznir, N. J. (2008). Lower-crustal intrusion on the North Atlantic continental margin. *Nature*, 452(7186), 460–464. <https://doi.org/10.1038/nature06687>
- Ziegler, P. A. (1992). European Cenozoic rift system. *Tectonophysics*, 208(1-3), 91–111. [https://doi.org/10.1016/0040-1951\(92\)90338-7](https://doi.org/10.1016/0040-1951(92)90338-7)